Ab initio investigation of high-entropy alloys of 3*d* elements

Fuyang Tian,[1,2] Lajos Karoly Varga,[3] Nanxian Chen,[2,4] Lorand Delczeg,[1] and Levente Vitos[1,3,5]

[1]*Applied Materials Physics, Department of Materials Science and Engineering, Royal Institute of Technology, Stockholm SE-100 44, Sweden*

[2]*Institute for Applied Physics, University of Science and Technology Beijing, Beijing 100083, China*

[3]*Wigner Research Centre for Physics, Institute for Solid State Physics and Optics, H-1525 Budapest, P.O. Box 49, Hungary*

[4]*Department of Physics, Tsinghua University, Beijing 100084, China*

[5]*Department of Physics and Astronomy, Division of Materials Theory, Uppsala University, Box 516, SE-751210 Uppsala, Sweden*

(Received 26 October 2012; published 26 February 2013)

Single-phase high-entropy alloys are investigated using the exact muffin-tin orbitals (EMTO) method in combination with the coherent potential approximation (CPA). Choosing the paramagnetic face-centered-cubic NiCoFeCr alloy as an example, we compare the CPA results with those obtained using the supercell (SC) method. For the equilibrium Wigner-Seitz radius and elastic properties, the single-site mean-field approximation turns out to yield consistent results with the SC approach. Next, we employ the EMTO-CPA method to study the bulk properties of $CuNiCoFeCrTi_x$ ($x = 0.0$–$0.5, 1.0$) and NiCoFeCrTi high-entropy alloys. A detailed comparison between the theoretical results and the available experimental data demonstrates that *ab initio* theory can properly describe the fundamental properties of this important class of engineering alloys. Theory predicts NiCoFeCr and CuNiCoFeCr to be more isotropic and less ductile than the Ti-containing single-phase alloys ($CuNiCoFeCrTi_x$ with $x \gtrsim 0.4$ and NiCoFeCrTi).

DOI: 10.1103/PhysRevB.87.075144 PACS number(s): 62.20.D−, 71.15.Nc, 71.20.Be

I. INTRODUCTION

In the early 2000s, a simple solid solution phase was discovered in the equimolar multicomponent alloys.[1,2] Yeh *et al*. named the new type of metals "high-entropy alloys" (HEAs). These metastable solid solutions are composed of at least five equimolar or near-equimolar metallic elements and are stabilized by the mixing entropy $\Delta S_{\mathrm{mix}} = k_B \ln n$ (k_B is the Boltzmann constant and n is the molar fraction of the equimolar alloy components).[1] Due to the unique microstructures and special properties, such as high strength, good wear, corrosion resistance, and oxidation, HEAs have attracted rapidly increasing attention in the scientific community.[3–26]

In the experimental area, researchers used different tools, including traditional casting, mechanical alloying, sputtering, and splat quenching, to obtain the HEAs with different alloying elements and then to investigate the corresponding microstructure and mechanical, thermal, and electronic performances.[3–18] With the appearance of a large number of different-type HEAs, one could establish general rules governing the physics of HEAs. Such empirical assessments were based on the regular solution theory, and made use of the atomic mismatch, mixing entropy and enthalpy, electronegativity, and valence electron concentration.[19–23]

On the other hand, atomistic simulation methods were applied to study the features connected to the microstructure of the HEAs. For instance, del Grosso *et al*. employed the Bozzolo-Ferrante-Smith (BFS) method for alloys to investigate the transition to the high-entropy regime for alloys with refractory elements.[24] Based on *ab initio* simulations combined with the supercell technique, it was reported that the body-centered-cubic (bcc) phase has partial ionic bonding between Al and other transition metals for the series of HEAs $Al_xCr_yCoNiFe$ ($x = 1, 1.5, 2, 2.5$, and 3, $y = 1$ and 2).[25] Zhang *et al*. used the sublattice model, supported by first-principles total energy calculations, to explore the possibility of forming face-centered-cubic (fcc) HEAs of CoFeMnNiM and CoFeMnNiSmM (M = Cr, Zn, Ru, Rh, Pd, Re, Os, Ir, and Pt).[26]

Despite of the single solid solution phase, characteristic to HEAs, it is particularly difficult to use conventional *ab initio* atomistic simulation methods to investigate these systems. That is because HEAs are chemically and often also magnetically disordered multicomponent extended solid solutions. In the present work, our primary goal is to assess the performance of standard alloy theory based on *ab initio* density functional theory[27,28] in the case of HEAs. To this end, we employ the exact muffin-tin orbitals (EMTO) method[29–34] in combination with the coherent potential approximation (CPA)[35–39] and investigate the basic bulk properties of a few selected HEAs based on 3*d* transition metals (abbreviated here "3*d*-HEAs"). Using NiCoFeCr as a four-component model system, first we establish the accuracy of the single-site mean-field approximation by comparing the CPA results with those generated by the supercell technique. In the second step, we extend our study to CuNiCoFeCr, NiCoFeCrTi, and $CuNiCoFeCrTi_x$ high-entropy alloys. Based on the calculated electronic structure, we give an explanation for the observed magnetic state. We provide the theoretical predictions for the elastic parameters and compare the calculated Young's moduli with the available experimental data for $CuNiCoFeCrTi_x$ ($x = 0.0$–$0.5, 1.0$) and NiCoFeCrTi. We also discuss the micromechanical properties of 3*d*-HEAs using the theoretical elastic moduli.

Today, no consistent notation for the chemical formula of the HEAs exists. One of the main characteristics of the HEAs is that all constituents have similar weights, so there are no solvent matrix and solute atoms. Hence, here we adopt a generally applicable convention based on the atomic numbers of the alloy components. According to that, the constituents are specified in order of their atomic numbers, starting from the left side with the element having the largest atomic number. With this convention, it is possible to put the common minor alloying elements (e.g., Ti or Al) to the end of the chemical formula.

The rest of the paper is organized as follows. In Sec. II, we present the theoretical tool and give the most important details of the numerical calculation. The results are presented and discussed in Sec. III, and the paper ends with conclusions.

II. METHODOLOGY

The EMTO method is an efficient and accurate method for solving the Kohn-Sham equations.[28] It uses large overlapping muffin-tin potential spheres which can describe the exact one-electron potential rather accurately. In the calculation of total energy, the EMTO method employs the full charge density (FCD) technique[30,33,34] which not only improves the calculation efficiency but also ensures total energies an accuracy similar to that of the full-potential methods. Today, the CPA represents the most efficient alloy theory for the electronic structure calculations in multicomponent random solid solutions.[35–39] The single-site nature of the CPA limits its applicability to systems with negligible short-range order and local lattice relaxation effects. Nevertheless, it turned out that the EMTO-CPA method can accurately capture the structural energy differences and trace energy changes related to lattice distortions in complex alloys.[40–45]

In the present EMTO calculations, we employed the Perdew-Burke-Ernzerhof (PBE) exchange-correlation approximation to obtain the charge density and total energy.[46] The Kohn-Sham equations were solved within the scalar-relativistic and soft-core approximations. The Green's function was calculated for 16 complex energy points distributed exponentially on a semicircular contour including the valence states. The EMTO basis set included s,p,d, and f states. We used 240 inequivalent $\mathbf{k}$ points in the irreducible wedge of the fcc Brillouin zone. The electrostatic correction to the single-site CPA was described using the screened impurity model[47] with screening parameter 0.6. For all alloy components, the potential sphere radii were chosen to be equal to the corresponding average atomic sphere radius. All calculations were performed for a static lattice, that is, neglecting all thermal contributions.

The equilibrium volumes (V) and bulk modulus (B) were extracted from the equation of state described by a Morse function[48] fitted to the total energy calculated for seven different volumes around the equilibrium. In this paper, the equilibrium volume is expressed in terms of average Wigner-Seitz radius w. In a cubic lattice there are three independent elastic constants, c_{11}, c_{12}, and c_{44}, which are connected to the bulk modulus $B=(c_{11}+2c_{12})/3$ and the tetragonal shear modulus $c'=(c_{11}-c_{12})/2$. The elastic anisotropy is given in terms of Zener ratio $A_Z=c_{44}/c'$. The two shear elastic parameters c' and c_{44} were computed according to the standard methodology from Ref. 39. Namely, we used the following volume conserving orthorhombic and monoclinic deformations:

$$\begin{pmatrix} 1+\delta_o & 0 & 0 \\ 0 & 1-\delta_o & 0 \\ 0 & 0 & \frac{1}{1-\delta_o^2} \end{pmatrix} \quad \text{and} \quad \begin{pmatrix} 1 & \delta_m & 0 \\ \delta_m & 1 & 0 \\ 0 & 0 & \frac{1}{1-\delta_m^2} \end{pmatrix}, \quad (1)$$

which lead to the energy change $\Delta E(\delta_o)=2Vc'\delta_o^2+O(\delta_o^4)$ and $\Delta E(\delta_m)=2Vc_{44}\delta_m^2+O(\delta_m^4)$. Both energies were computed for six distortions, $\delta=0.00,0.01,\ldots,0.05$. An isotropic polycrystalline system is described by the bulk modulus B and the shear modulus G. For a cubic lattice, the polycrystalline bulk modulus is identical with the single-crystal bulk modulus. For the shear modulus, we used the arithmetic Hill average $G=(G_R+G_V)/2$ of the Voigt and Reuss bounds given by[49]

$$G_R=\frac{5(c_{11}-c_{12})c_{44}}{4c_{44}+3(c_{11}-c_{12})} \quad \text{and} \quad G_V=\frac{c_{11}-c_{12}+3c_{44}}{5}. \quad (2)$$

These two bounds may be used to compute the ratio $A_{VR}=(G_V-G_R)/(G_V+G_R)$, which is used as another measure of the elastic anisotropy. Elastically isotropic materials have $A_{VR}=0$ and $A_Z=1$. The Young's modulus E and Poisson ratio ν are connected to B and G by the relations

$$E=\frac{9BG}{3B+G} \quad \text{and} \quad \nu=\frac{3B-2G}{2(3B+G)}. \quad (3)$$

We note that large A_{VR} indicates large uncertainty in the predicted shear and Young's moduli and Poisson ration.

Experiments indicate that NiCoFeCr, NiCoFeCrTi, CuNiCoFeCr, and $CuNiCoFeCrTi_{0.5}$ are paramagnetic (PM) metals and $CuNiCoFeCrTi_{1.0}$ is superparamagnetic.[5,9,10] For $CuNiCoFeCrTi_x$ ($x\leqslant 1$) the magnetic transition temperature was reported to be below 170 K.[5] Here we employed the disordered local magnetic moment (DLM) picture[50–53] to describe the paramagnetic state of these HEAs. The DLM model was shown to correctly account for the random distribution of the local magnetic moments of the PM state of metals well above the magnetic transition temperature, where the magnetic moments show negligible short-range order.[43,54–56] According to that model, an alloy component M of concentration m is presented by its spin-up ($\uparrow$) and spin-down ($\downarrow$) counterparts assumed to be distributed randomly on the underlying sublattice; i.e., each magnetic alloy component is treated as $M_m \rightarrow M^{\uparrow}_{m/2}M^{\downarrow}_{m/2}$. For example, NiCoFeCr is described as a quasi-eight-component random solid solution, viz., $Fe^{\uparrow}_{0.125}Fe^{\downarrow}_{0.125}$ $Cr^{\uparrow}_{0.125}Cr^{\downarrow}_{0.125}$ $Ni^{\uparrow}_{0.125}Ni^{\downarrow}_{0.125}Co^{\uparrow}_{0.125}Co^{\downarrow}_{0.125}$.

III. RESULTS

A. Coherent potential approximation versus supercell technique

In order to assess the performance of CPA in the case of HEAs, we selected NiCoFeCr and set up a simple supercell (SC) with fcc underlying lattice. To mimic a homogeneous solid solution, we distributed the four alloying elements so that they are neighbors to each other within a conventional fcc unit cell, as shown in Fig. 1. Similar structures for the HEAs were suggested in Refs. 57 and 58. We notice that in contrast to the present model structure from Fig. 1, NiCoFeCr was found to show no tendency for long-range ordering.[58] However, taking into account that the long-range order has a rather small effect on the elastic properties of alloys,[59] a direct comparison between the CPA and the SC results calculated for the present ordered structure seems to be appropriate.

The results obtained for the supercell from Fig. 1 and those calculated for the corresponding $Ni_{0.25}Co_{0.25}Fe_{0.25}Cr_{0.25}$ random solid solution are listed in Table I. The SC equilibrium Wigner-Seitz radius is 2.601 bohrs, which is rather close to 2.607 bohrs obtained for the solid solution using CPA. The

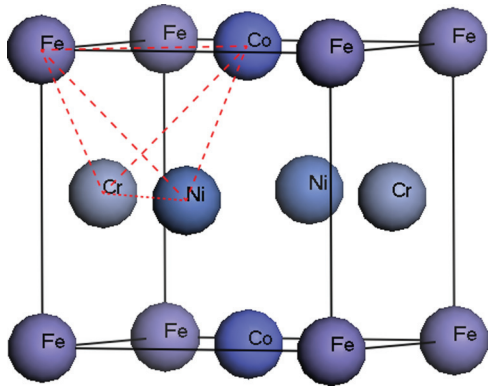

FIG. 1. (Color online) The supercell used to model the NiCoFeCr alloy (Ref. 58).

agreement between the SC (207 GPa) and CPA (208 GPa) bulk moduli is also excellent. For all theoretical parameters, we find a good consistency between the CPA and SC results. In particular, the three cubic elastic constants, c_{11}, c_{12}, and c_{44}, obtained with the two methods differ on the average by ∼4%. The somewhat larger relative errors in the Zener anisotropy (c_{44}/c') and the Cauchy pressure ($c_{12} - c_{44}$) are still acceptable, especially if we consider that the present supercell is the simplest periodic approximant of the four-component random alloy considered in the CPA calculations. The good agreement seen for the shear and Young's modulus, the Poisson ratio, and the polycrystalline anisotropy ratio indicates that the CPA is an efficient and accurate method to investigate the bulk properties of these multicomponent alloys.

B. Equilibrium volume

We compare the present *ab initio* Wigner-Seitz radii calculated for NiCoFeCr, CuNiCoFeCr, and NiCoFeCrTi with the available experimental values measured by x-ray diffraction in Table II. In general, the two sets of data are in good agreement with each other, the average relative deviation between theory and experiment being below 1%. Furthermore, adding the equimolar Cu to NiCoFeCr increases the radius from 2.607 bohrs to 2.628 bohrs, which is in line with the experimental observation.

In Table II, we list the PBE-level results from Ref. 39 as well as some experimental data for the elementary solids in their low-temperature crystallographic phases. It has been found that density functional theory (PBE level) underestimates the equilibrium volume of hexagonal-close-packed (hcp) Ti, antiferromagnetic B2 Cr, ferromagnetic body-centered-cubic (bcc) Fe, ferromagnetic hcp Co, and fcc Ni, whereas for fcc Cu a weak underbinding is observed.[39] Using the Wigner-Seitz radii for the alloy constituents, we may estimate the equilibrium volume of the HEAs via Vegard's rule. In Table II, $\overline{w}_c$ stands for the estimated volume based on the quoted PBE-level theoretical data, and $\overline{w}_e$ the one obtained from the experimental data.

TABLE I. Theoretical bulk parameters for fcc NiCoFeCr alloy calculated using the CPA and SC approximations. Listed are the equilibrium Wigner-Seitz radius w (bohrs), cubic elastic constants c_{11}, c_{12}, and c_{44}, and c' (GPa), the Zener anisotropy A_Z, the Cauchy pressure ($c_{12} - c_{44}$) (GPa), the bulk modulus B (GPa), the shear modulus G (GPa), the Young modulus E (GPa), the Poisson ration ν, and the polycrystalline elastic anisotropy ratio A_{VR}.

Method	c_{11}	c_{12}	c_{44}	c'	A_Z	$(c_{12} - c_{44})$
CPA	271.0	175.0	189.3	48.0	3.9	−14.3
SC	257.1	183.5	193.9	36.8	5.2	−10.4
	w	B	G	E	ν	A_{VR}
CPA	2.607	207	110	280	0.275	0.21
SC	2.601	208	101	262	0.290	0.29

Rather interestingly, $\overline{w}_e$ gives an excellent estimate for the equilibrium radius of NiCoFeCr and CuNiCoFeCr alloys. However, for NiCoFeCrTi, the experimental value is 2.7% smaller than the one obtained from the linear mixing of the radii of the alloy components. Such a large deviation from Vegard's rule is somewhat unexpected especially in the mirror of the other two cases. Most recent experiments[10,60] showed that the as-cast NiCoFeCrTi alloy contains two minor phases in addition to the main fcc matrix. We speculate that the presence of the bcc α-Fe-Cr solid solution and the $CoTi_2$ intermetallic compound might be the reason for the above discrepancy. Furthermore, comparing $\overline{w}_c$ to $\overline{w}_e$, we observe a systematic underestimation of the equilibrium volume by the theory. Similar deviations are found between w(EMTO) and w(Expt.) for NiCoFeCr and CuNiCoFeCr but not for NiCoFeCrTi. Therefore, we conclude that the apparent underbinding by the PBE-level density functional theory in the case of NiCoFeCrTi is not realistic, and the present experimental volume may not represent the correct equilibrium volume of a metastable fcc NiCoFeCrTi solid solution. Assuming a systematic error in the theoretical equilibrium volume, we estimate that the true equilibrium Wigner-Seitz radius of fcc NiCoFeCrTi solid solution should be somewhere around 2.70 bohrs.

The calculated equilibrium radii of $NiCoFeCrTi_x$ (x = 0.1–0.5,1.0) are shown in Fig. 5 (upper panel) and listed in Table III as a function of x. It is found that Ti addition gradually increases the equilibrium volume of CuNiCoFeCr, in line with the result obtained for NiCoFeCr and NiCoFeCrTi (Table II).

C. Magnetic structure

Figure 2 shows the local magnetic moments (↑ or ↓) versus the Wigner-Seitz radius for the magnetic sublattices in paramagnetic CuNiCoFeCr, NiCoFeCr, and NiCoFeCrTi high-entropy alloys. According to the present calculations, the local magnetic moments vanish on the Ni, Cu, and Ti sites for all volumes and thus they are not shown in the figure. We should note that thermal effects would eventually induce local magnetic moments on the Ni sites as well at finite temperature. Such longitudinal spin fluctuations have been neglected in the present study. For all alloys, Fe possesses a significant [∼(1.8–2.0)μ_B] local magnetic moment around the equilibrium volume. Cobalt remains nonmagnetic in NiCoFeCr and NiCoFeCrTi but shows a small (∼0.6μ_B) magnetic moment for CuNiCoFeCr.

In order to understand the magnetic state of the present 3d-HEAs, we investigate the electronic structure of the hypothetical nonmagnetic and paramagnetic fcc solid solutions. The nonmagnetic total density of states (DOS) and partial

TABLE II. Theoretical (EMTO) and experimental (Expt.) Wigner-Seitz radii (in bohrs) for NiCoFeCr, CuNiCoFeCr, and NiCoFeCrTi HEAs. For reference, former theoretical (PBE level, w_c) and experimental (w_e) radii for the elementary solids in their ground-state crystallographic structures (indicated in parentheses) are also listed (Ref. 39). Δ is the relative difference between w(EMTO) and w(Expt.). $\overline{w}_c$ and $\overline{w}_e$ represent the alloys' Wigner-Seitz radii as estimated from the quoted w_c and w_e values, respectively, according to Vegard's rule.

HEAs	str.	w(EMTO)	w(Expt.)	Δ	$\overline{w}_c$	$\overline{w}_e$
NiCoFeCr	fcc	2.607	2.632[9]	0.95%	2.623	2.642
CuNiCoFeCr	fcc	2.628	2.643[5]	0.57%	2.636	2.647
NiCoFeCrTi	fcc	2.682	2.650[7]	1.21%	2.706	2.724
Element	Ti (hcp)	Cr (B2)	Fe (bcc)	Co (hcp)	Ni (fcc)	Cu (fcc)
w_c	3.04	2.65	2.64	2.60	2.60	2.69
w_e	3.053	2.684	2.667	2.613	2.602	2.669

density of states (pDOS) for CuNiCoFeCr, NiCoFeCr, and NiCoFeCrTi are plotted in Fig. 3. All DOS calculations were done at the proper theoretical equilibrium volume.

We observe that in spite of the compositional disorder, all alloys have a rather structured DOS with a substantial peak just below the Fermi level (E_F). This peak is mainly due to the peaks in the pDOS of Co and Ni and to some extent also Fe. The size of the total DOS at E_F [$D(E_F)$] decreases when adding Cu or Ti to the host composition. This DOS decrease is primarily due to the 5% drop in the atomic fractions for Fe, Co, Cr, and Ni, which cannot be compensated by the relatively low pDOS of Cu and Ti near E_F. In nonmagnetic alloys, the major peaks in the pDOS are located above the Fermi level for Ti and Cr and below the Fermi level for Co, Ni, and Cu. This can be explained by simple band filling arguments considering that all alloy components experience the same fcc environment.

For all alloys, Fe has a moderate pDOS peak located very close to the Fermi level. It is found that $D_{\mathrm{Fe}}(E_F)$ is the largest among all pDOS at E_F, followed by $D_{\mathrm{Co}}(E_F)$ and $D_{\mathrm{Cr}}(E_F)$. This distinct Fe peak at E_F leads to magnetic instability in Fe sublattice, and in turn to finite spin polarization on Fe atoms. In Fig. 4, we show the spin-polarized pDOS for $\mathrm{Fe}^{\uparrow}$, $\mathrm{Co}^{\uparrow}$, and $\mathrm{Cr}^{\uparrow}$. We note that the pDOS for $\mathrm{Fe}^{\downarrow}$, $\mathrm{Co}^{\downarrow}$, and $\mathrm{Cr}^{\downarrow}$ are identical to those shown in the figure (apart from the sign). As seen in Fig. 4, the spin-polarized Fe pDOS has two separate peaks: one above the Fermi level and one below the Fermi level. These two Fe peaks hybridize with the Cr and Co peaks, respectively. As a result of the magnetic splitting, the total $D(E_F)$ drops significantly in all three alloys. In nonmagnetic CuNiCoFeCr (Fig. 3), we have $D_{\mathrm{Fe}}(E_F) \approx D_{\mathrm{Co}}(E_F)$ and the Co peak is close to E_F. This explains the appearance of the local magnetic moments on the Co sites in the paramagnetic CuNiCoFeCr.

Additional total energy calculations performed for the hypothetical nonmagnetic fcc $3d$-HEAs give 2.592 bohrs, 2.610 bohrs, and 2.675 bohrs for the equilibrium Wigner-Seitz radii of NiCoFeCr, CuNiCoFeCr, and NiCoFeCrTi, respectively. These values are smaller than those listed in Table II, which were obtained for the paramagnetic state. Taking into account the uncertainty associated with the experimental equilibrium volume of NiCoFeCrTi (Sec. III B), we may conclude that neglecting the paramagnetism in the present $3d$-HEAs worsens the agreement between theory and experiment for the equation of state.

D. Cubic elastic constants

The three cubic elastic constants c_{11}, c_{12}, and c_{44} as well as the c', c_{44}/c', and $(c_{12} - c_{44})$ of NiCoFeCr, CuNiCoFeCrTi$_x$, and NiCoFeCrTi are listed in Table III. The results for CuNiCoFeCrTi$_x$ are also plotted in Fig. 5 as a function of Ti content. Unfortunately, we could not find any published

TABLE III. Theoretical Wigner-Seitz radius w (bohrs), elastic constants c_{11}, c_{12}, and c_{44} as well as c', c_{44}/c', and $(c_{12} - c_{44})$, elastic moduli B, G, and E, and Poisson ratio ν for paramagnetic fcc NiCoFeCr, CuNiCoFeCrTi$_x$ (x = 0.0–0.5, 1.0), and NiCoFeCrTi alloys. For reference, the available experimental Young's moduli are also listed.

x	w	c_{11}	c_{12}	c_{44}	c'	A_Z	$(c_{12} - c_{44})$	B	G	B/G	A_{VR}	ν	E	E(Expt.)
							NiCoFeCr							
	2.607	271.0	175.0	189.3	48.0	3.9	−14.3	207	110	1.88	0.21	0.275	280.0	
							CuNiCoFeCrTi$_x$							
0	2.628	227.8	154.6	165.3	36.6	4.6	−10.7	179	91	1.97	0.25	0.282	234.0	55.6[5]
0.1	2.635	219.7	152.6	160.2	33.5	4.8	−7.5	175	87	2.01	0.26	0.288	223.1	
0.2	2.643	213.6	152.1	155.1	30.5	5.1	−3.0	173	82	2.10	0.28	0.294	213.1	
0.3	2.651	209.6	151.9	154.6	28.9	5.3	−2.2	172	80	2.15	0.30	0.298	205.9	
0.4	2.655	207.6	151.7	150.8	27.9	5.4	2.0	171	78	2.19	0.31	0.303	200.4	
0.5	2.663	198.4	151.0	142.7	23.7	6.0	8.3	169	71	2.38	0.34	0.313	187.1	98.6[5]
1.0	2.694	174.3	148.6	125.0	12.8	9.8	23.6	157	54	2.91	0.48	0.346	145.4	76.5[5]
							NiCoFeCrTi							
	2.682	184.5	170.9	127.0	6.8	18.7	43.9	175	47	3.72	0.67	0.376	130.3	134[7]

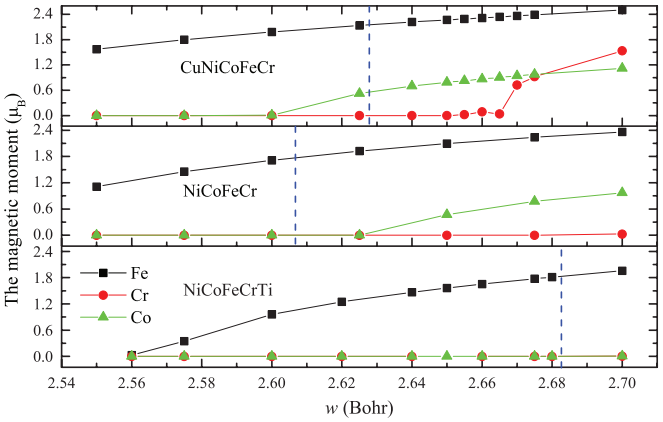

FIG. 2. (Color online) Local magnetic moments of Fe, Cr, and Co in paramagnetic fcc NiCoFeCr, CuNiCoFeCr, and NiCoFeCrTi alloys as a function of the Wigner-Seitz radius. For each alloy, the vertical (blue) line represents the calculated equilibrium Wigner-Seitz radius.

experimental data on the single-crystal elastic parameters of these 3*d*-HEAs.

As seen from Table III, all 3*d*-HEAs considered here are mechanically stable. That is, for all alloys the single-crystal elastic constants satisfy the $c_{44} > 0, c_{11} > |c_{12}|$, and $c_{11} + 2c_{12} > 0$ dynamical stability conditions.[49] Titanium decreases the tetragonal elastic constant c' both in NiCoFeCrTi and CuNiCoFeCrTi$_x$, as compared to that of NiCoFeCr. This indicates that Ti decreases the mechanical stability of the fcc phase, which is in line with the expectation based on the effective number of *d* electrons.

Theory predicts a moderate elastic anisotropy and negative Cauchy pressure for NiCoFeCr. Negative $(c_{12} - c_{44})$ has been associated with the covalent nature of the metallic bond and is characteristic of brittle alloys.[61] In lack of any

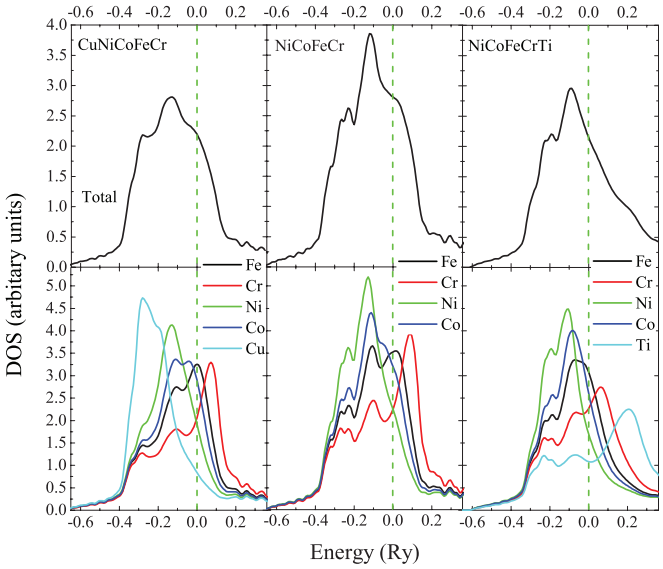

FIG. 3. (Color online) Total (upper panels) and partial (lower panels) density of states for the nonmagnetic fcc CuNiCoFeCr, NiCoFeCr, and NiCoFeCrTi alloys. The position of the Fermi level is marked by vertical dashed lines.

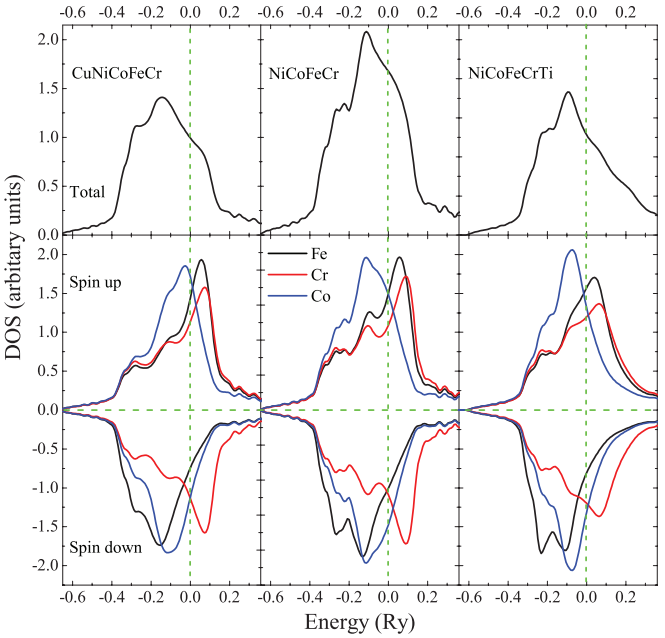

FIG. 4. (Color online) Total (upper panels) and Fe, Co, and Cr partial (lower panels) density of states for the paramagnetic fcc CuNiCoFeCr, NiCoFeCr, and NiCoFeCrTi alloys. In the lower panels, only the Fe$^{\uparrow}$, Co$^{\uparrow}$, and Cr$^{\uparrow}$ partial densities of states are shown. Apart from the sign (spin up vs spin down) difference, the partial densities of states for Fe$^{\downarrow}$, Co$^{\downarrow}$, and Cr$^{\downarrow}$ are identical to those shown in the figure.

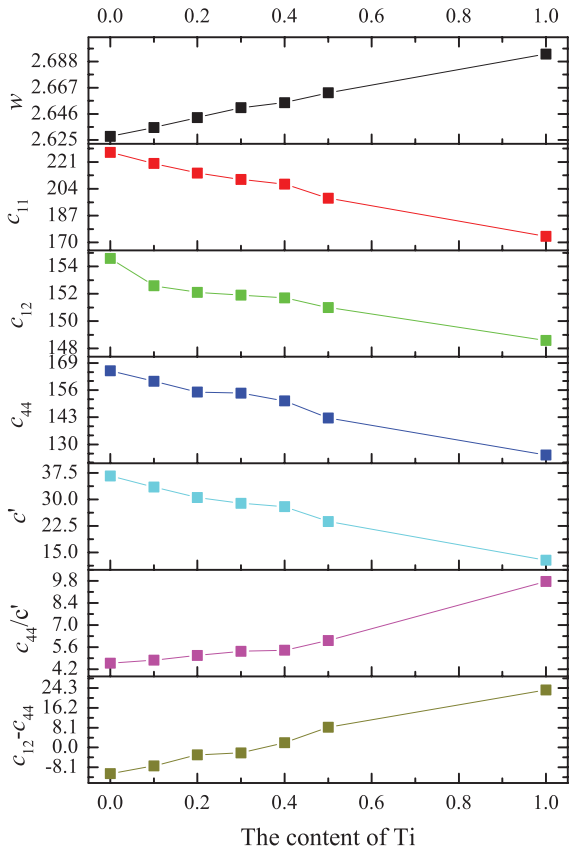

FIG. 5. (Color online) Elastic constants and equilibrium Wigner-Seitz radius calculated for paramagnetic fcc CuNiCoFeCr and CuNiCoFeCrTi$_x$ ($x = 0.1$–$0.5, 1.0$) alloys.

experimental data, we compare the present results calculated for paramagnetic NiCoFeCr with those obtained for paramagnetic austenitic stainless steel alloys composed of ∼18% Cr, ∼8% Ni, and balance Fe.[62] The three cubic elastic constants reported for this stainless steel are $c_{11} = 208.6$ GPa, $c_{12} = 143.5$ GPa, and $c_{44} = 132.8$ GPa, which yield 4.07 for the Zener anisotropy ratio and 10.7 GPa for the Cauchy pressure. Therefore, compared to the austenitic stainless steels, the paramagnetic NiCoFeCr is predicted to be less ductile. Equimolar Cu addition to NiCoFeCr is found to increase slightly the Cauchy pressure from −14.3 GPa obtained for NiCoFeCr to −10.7 GPa calculated for CuNiCoFeCr. For reference, fcc Ir has Cauchy pressure of −13 GPa, and undergoes both transgranular and intergranular fracture.[61]

Titanium is found to change the NiCoFeCr host into a ductile but strongly anisotropic material. Equimolar fcc NiCoFeCrTi has $c_{44}/c' = 18.7$ and $(c_{12} - c_{44}) = 43.9$ GPa. Such high anisotropy ratio is rather unusual. For comparison, the Zener anisotropy of paramagnetic body-centered-cubic (bcc) and fcc Fe was found to be around 8.6 and 3.6, respectively.[54] Considering the change of the Cauchy pressure upon equimolar doping, we may conclude that although Cu also improves the ductility of the 3*d*-HEAs, Ti makes it especially ductile. Indeed, as seen in the case of CuNiCoFeCrTi$_x$, Ti can remedy the large negative Cauchy pressure of the host alloy. It gradually increases the metallic character of the bonds turning $(c_{12} - c_{44})$ positive somewhere between $x = 0.3$ and $x = 0.4$. We find that all elastic parameters of CuNiCoFeCrTi$_x$ change monotonously with the amount of Ti (Fig. 5). According to the present theoretical calculations, the bulk parameters of single-crystal CuNiCoFeCrTi$_{0.5}$ HEAs, which are still believed to be single-phase alloys, are surprisingly close to those reported for the Fe$_{0.74}$Cr$_{0.18}$Ni$_{0.08}$ austenitic stainless steel alloy.[62]

E. Polycrystalline elastic moduli

The polycrystalline elastic moduli B, G, E, and ν of NiCoFeCr, CuNiCoFeCrTi$_x$, and NiCoFeCrTi are listed in Table III. The theoretical values for CuNiCoFeCrTi$_x$ are also plotted in Fig. 6 as a function of Ti content. The experimental information on the polycrystalline elastic moduli is also very limited, the only available data being the Young's modulus for NiCoFeCrTi and CuNiCoFeCrTi$_x$ with $x = 0,0.5$, and 1.0.[5,7]

The bulk modulus, shear modulus, and Young's modulus follow similar trends as those seen for the single-crystal elastic parameters. The polycrystalline elastic anisotropy A_{VR} increases from ∼0.25 in CuNiCoFeCr to ∼0.49 in CuNiCoFeCrTi. A significant increase of the Poisson ratio with x is found.

The changes in the B/G ratio correlate reasonably well with those found for the Cauchy pressure. B/G is often used as an indicator of the brittle-ductile behavior.[63] It was proposed that a material is ductile when its B/G ratio is greater than 1.75; otherwise it is in the brittle regime. According to Table III, the B/G ratios of NiCoFeCr and CuNiCoFeCr are close to the above critical value, and Ti addition brings both of these fcc alloys well into the ductile regime. We should note, however, that based merely on the Pugh criteria,[63] all alloys considered here are predicted to be ductile (i.e., possess $B/G > 1.75$).

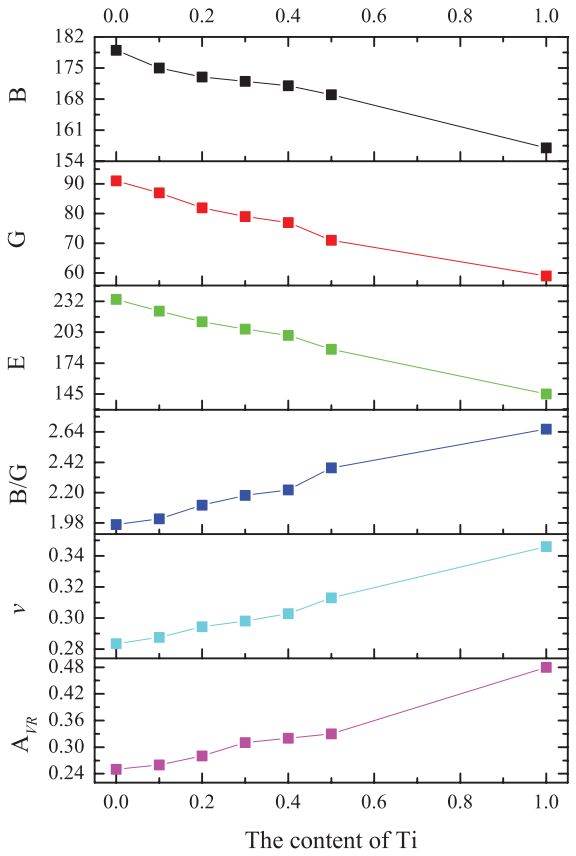

FIG. 6. (Color online) Elastic moduli calculated for paramagnetic fcc NiCoFeCr and CuNiCoFeCrTi$_x$ ($x = 0.1$–$0.5, 1.0$) alloys.

Bulk metallic glasses (BMGs) with Poisson ratio larger than ∼0.31 were reported to be ductile. In particular, a very clear onset of plasticity was observed in Fe$_{65}$Mo$_{14}$C$_{15}$B$_6$ bulk amorphous steel doped with lanthanides as the Poissons ratio approached 0.31–0.32 from below.[64] The bulk, shear, and Young's moduli of Fe$_{65-x}$Mo$_{14}$C$_{15}$B$_6$Er$_x$ vary with the amount of Er within ∼176–196 GPa, ∼73–77 GPa, and ∼192–202 GPa, respectively. These values are relatively close to those predicted by the present theory for CuNiCoFeCrTi$_x$ HEAs (Table III), and thus a direct comparison of the Poisson ratio of HEAs to that of BMGs may also be appropriate. Considering the composition dependence of the Poisson ratio of the present HEAs, we find that $\nu(x)$ reaches the critical value of 0.31 just around $x = 0.4$, where the Cauchy pressure becomes positive.

Next we compare the theoretical results with the available experimental data. It is particularly surprising that for CuNiCoFeCr, our Young's modulus of 234 GPa is about four times larger than 55.6 GPa found in experiment.[5] This alloy shows relatively low anisotropy and thus the uncertainty associated with the Voigt-Reuss-Hill averaging are expected to be small. Furthermore, as shown in Fig. 7, the Young's modulus of a single-crystal CuNiCoFeCr changes between 102.79 GPa obtained for the ⟨001⟩ direction and 379.18 GPa calculated for the ⟨111⟩ direction. Therefore, even for a highly textured material, theory would predict the lowest E to be around 100 GPa, which is still almost double the experimental value. For the two Ti-containing CuNiCoFeCrTi$_{0.5}$ and CuNi-

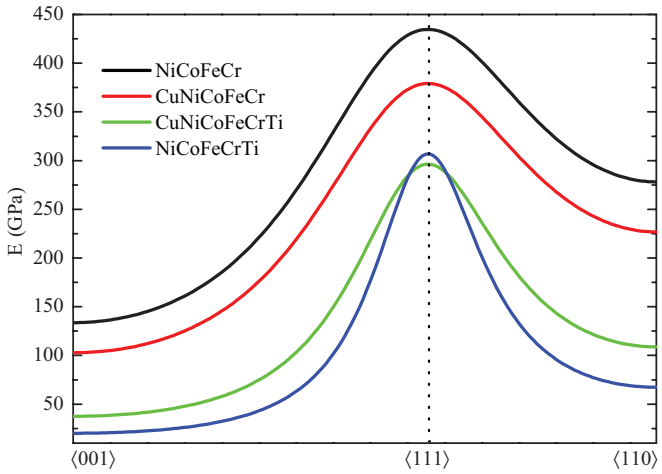

FIG. 7. (Color online) Theoretical Young's modulus for NiCoFeCr, CuNiCoFeCr, CuNiCoFeCrTi, and NiCoFeCrTi alloys plotted in plane (110) as a function of direction, including the three main cubic directions.

CoFeCrTi alloys the calculated Young's moduli differ from the reported experimental values by ∼90%. On the other hand, the agreement between theory and experiment is almost perfect for NiCoFeCrTi. Such good agreement is rather unexpected since for this alloy we obtained very large anisotropy ratio. The single-crystal Young's modulus of NiCoFeCrTi changes significantly with direction (Fig. 7), the lowest value being close to 20 GPa (for ⟨001⟩) and the largest around 307 GPa (for ⟨111⟩). Moreover, recent experiments show that NiCoFeCrTi is not even a single fcc phase alloy.[60]

As one possible reason for the above difference between theory and experiment, we should mention that all present calculations were carried out at static conditions (0 K), while the experimental measurements were performed at room temperature. In addition, our calculations assumed an ideal solid solution phase with fcc underlying lattice in contrast to the real alloys having complex microstructure. For instance, in CuNiCoFeCr, Cu segregation to the interdendrite region was observed.[4] We should also point out that for some other HEAs, the experimental values for the Young's modulus differ significantly. For example, for $NiCoFeCrAlTi_{0.5}$ the measured E varies between 72.68 GPa (Ref. 65) and 177.7 GPa (Ref. 66). On this ground, the reliability of the measured Young's modulus for $CoNiCoFeCrTi_x$ may also be questionable, especially given that no important experimental details are given in Ref. 5.

IV. CONCLUSIONS

We employed the EMTO-CPA method to investigate the electronic structure and basic bulk properties of NiCoFeCr, CuNiCoFeCr, $CuNiCoFeCrTi_x$, and NiCoFeCrTi 3d-HEAs. In all calculations, it was assumed that the above alloys are single-phase paramagnetic face-centered-cubic random solid solutions. The relatively good agreement between the calculated and measured equilibrium volumes for the NiCoFeCr, CuNiCoFeCr, and NiCoFeCrTi alloys demonstrates that alloy theory is able to describe these complex multicomponent paramagnetic alloys.

We have shown that with increasing Ti amount in $CuNiCoFeCrTi_x$, the equilibrium Wigner-Seitz radius increases and the elastic constants decrease. Titanium is predicted to increase the elastic anisotropy of the single phase fcc $CuNiCoFeCrTi_x$ alloys and turn them more ductile compared to the other alloys considered here. In particular, the Ti-free alloys are calculated to have reduced ductility, as indicated by their negative Cauchy pressure and small Poisson ratio, whereas their theoretical B/G ratios suggest a ductile behavior. The obtained large deviation between the theoretical and experimental Young's modulus for some of the present alloys calls for more extensive experimental as well as theoretical studies on these important category of engineering materials.

ACKNOWLEDGMENTS

Work supported by the Swedish Research Council, the European Research Council, and the China Scholarship Council. The National 973 Project of China (Grant No. 2011CB606401) and the Hungarian Scientific Research Fund (OTKA 84078) are also acknowledged for financial support.

[1] J. W. Yeh, S. K. Chen, S. J. Lin, J. Y. Gan, T. S. Chin, T. T. Shun, C. H. Tsau, and S. Y. Chang, Adv. Eng. Mater. **6**, 299 (2004).
[2] B. Cantor, I. T. H. Chang, P. Knight, and A. J. B. Vincent, Mater. Sci. Eng. A **375**, 213 (2004).
[3] J. W. Yeh, S. K. Chen, J. Y. Gan, S. J. Lin, T. S. Chin, T. T. Shun, C. H. Tsau, and S. Y. Chang, Metall. Mater. Trans. A **35**, 2533 (2004).
[4] C. J. Tong, M. R. Chen. S. K. Chen, J. W. Yeh, T. T. Shun, S. J. Lin, and S. Y. Chang, Metall. Mater. Trans. A **36**, 1263 (2005).
[5] X. F. Wang, Y. Zhang, Y. Qiao, and G. L. Chen, Intermetallics **15**, 357 (2007).
[6] C. Li, J. C. Li, M. Zhao, and Q. Jiang, J. Alloys Compd. **475**, 752 (2009).
[7] K. B. Zhang, Z. Y. Fu, J. Y. Zhang, W. M. Wang, H. Wang, Y. C. Wang, Q. J. Zhang, and J. Shi, Mater. Sci. Eng. A **508**, 214 (2009).
[8] S. Singh, N. Wanderka, B. S. Murty, U. Glatzel, and J. Banhart, Acta Mater. **59**, 182 (2011).
[9] M. S. Lucas, L. Mauger, J. A. Munoz, Y. M. Xiao, A. O. Sheets, S. L. Semiatin, J. Horwath, and Z. Turgut, J. Appl. Phys. **109**, 07E307 (2011).
[10] K. B. Zhang and Z. Y. Fu, Intermetallics **28**, 34 (2012).
[11] S. Varalakshmi, G. A. Rao, M. Kamaraj, and B. S. Murty, J. Mater. Sci. **45**, 5158 (2010).
[12] Y. P. Wang, D. Y. Li, L. Parent, and H. Tian, Wear **271**, 1623 (2011).
[13] O. N. Senkov, G. B. Wilks, D. B. Miracle, C. P. Chuang, and P. K. Liaw, Intermetallics **18**, 1758 (2010).
[14] O. N. Senkov, J. M. Scott, S. V. Senkova, D. B. Miracle, and C. F. Woodward, J. Alloys Compd. **509**, 6043 (2011).
[15] X. Yang, Y. Zhang, and P. K. Liaw, Procedia Engineering **36**, 292 (2012).

[16]W. Y. Tang, M. H. Chuang, S. J. Lin, and J. W. Yeh, Metall. Mater. Trans. A **43**, 2390 (2012).
[17]S. K. Chen and Y. F. Kao, AIP Advances **2**, 012111 (2012).
[18]A. Cunliffe, J. Plummer. I. Figueroa, and I. Todd, Intermetallics **23**, 204 (2012).
[19]Y. Zhang, Y. J. Zhou, J. P. Lin, G. L. Chen, and P. K. Liaw, Adv. Eng. Mater. **10**, 534 (2008).
[20]Y. J. Zhou, Y. Zhang, F. J. Wang, and G. L. Chen, Appl. Phys. Lett. **92**, 241917 (2008).
[21]S. Guo, C. Ng, J. Lu, and C. T. Liu, J. Appl. Phys. **109**, 103505 (2011).
[22]S. Guo and C. T. Liu, Progress in Natural Science: Materials International **21**, 433 (2011).
[23]X. Yang and Y. Zhang, Mater. Chem. Phys. **132**, 233 (2012).
[24]M. F. del Grosso, G. Bozzolo, and H. O. Mosca, J. Alloys Compd. **534**, 25 (2012); Physica B: Condensed Matter **407**, 3285 (2012).
[25]C. Li, M. Zhao, J. C. Li, and Q. Jiang, J. Appl. Phys. **104**, 113504 (2008).
[26]C. Zhang, M. Lin, B. Wu *et al*. J. Shanghai Jiaotong Univ. (Sci.) **16**, 173 (2011).
[27]P. Hohenberg and W. Kohn, Phys. Rev. **136**, B864 (1964).
[28]W. Kohn and L. J. Sham, Phys. Rev. **140**, A1133 (1965).
[29]O. K. Andersen, O. Jepsen, and G. Krier, in *Lectures on Methods of Electronic Structure Calculation* (World Science, Singapore, 1994), p. 63.
[30]L. Vitos, Phys. Rev. B **64**, 014107 (2001).
[31]L. Vitos, H. L. Skriver, B. Johansson, and J. Kollár, Comput. Mater. Sci. **18**, 24 (2000).
[32]J. Kollár, L. Vitos, and H. L. Skriver, in *Electronic Structure and Physical Properties of Solids*, edited by H. Dreyssé, Lecture Notes in Physics (Springer-Verlag, Berlin, 2000).
[33]J. Kollár, L. Vitos, and H. L. Skriver, Phys. Rev. B **49**, 11288 (1994).
[34]L. Vitos, J. Kollár, and H. L. Skriver, Phys. Rev. B **49**, 16694 (1994); **55**, 13521 (1997).
[35]G. M. Stocks, W. M. Temmerman, and B. L. Gyorffy, Phys. Rev. Lett. **41**, 339 (1978).
[36]D. D. Johnson, D. M. Nicholson, F. J. Pinski, B. L. Gyorffy, and G. M. Stocks, Phys. Rev. Lett. **56**, 2088 (1986).
[37]L. Vitos, I. A. Abrikosov, and B. Johansson, Phys. Rev. Lett. **87**, 156401 (2001).
[38]B. L. Gyorffy, Phys. Rev. B **5**, 2382 (1972); P. Soven, Phys. Rev. **156**, 809 (1967).
[39]L. Vitos, *The EMTO Method and Applications in Computational Quantum Mechanics for Materials Engineers* (Springer-Verlag, London, 2007).
[40]L. Vitos, P. A. Korzhavyi, and B. Johansson, Phys. Rev. Lett. **88**, 155501 (2002).
[41]A. Taga, L. Vitos, B. Johansson, and G. Grimvall, Phys. Rev. B **71**, 014201 (2005).
[42]L. Huang, L. Vitos, S. K. Kwon, B. Johansson, and R. Ahuja, Phys. Rev. B **73**, 104203 (2006).
[43]L. Vitos, P. A. Korzhavyi, and B. Johansson, Phys. Rev. Lett. **96**, 117210 (2006).
[44]L. Vitos and B. Johansson, Phys. Rev. B **79**, 024415 (2009).
[45]H. Zhang, M. P. J. Punkkinen, B. Johansson, S. Hertzman, and L. Vitos, Phys. Rev. B **81**, 184105 (2010).
[46]J. P. Perdew, K. Burke, and M. Ernzerhof, Phys. Rev. Lett. **77**, 3865 (1996); **78**, 1396(E) (1997).
[47]P. A. Korzhavyi, A. V. Ruban, I. A. Abrikosov, and H. L. Skriver, Phys. Rev. B **51**, 5773 (1995).
[48]V. L. Moruzzi, J. F. Janak, and K. Schwarz, Phys. Rev. B **37**, 790 (1988).
[49]G. Grimvall, *Thermophysical Properties of Materials* (North-Holland, Amsterdam, 1999).
[50]B. L. Györffy, A. J. Pindor, J. Staunton, G. M. Stocks, and H. Winter, J. Phys. F **15**, 1337 (1985).
[51]T. Oguchi, K. Terakura, and N. Hamada, J. Phys. F **13**, 145 (1983).
[52]F. J. Pinski, J. Staunton, B. L. Györffy, D. D. Johnson, and G. M. Stocks, Phys. Rev. Lett. **56**, 2096 (1986).
[53]J. Staunton, B. L. Györffy, A. J. Pindor, G. M. Stocks, and H. Winter, J. Magn. Magn. Mater. **45**, 15 (1984).
[54]H. Zhang, B. Johansson, and L. Vitos, Phys. Rev. B **84**, 140411(R) (2011).
[55]D. Music, T. Takahashi, L. Vitos, C. Asker, I. A. Abrikosov, and J. M. Schneider, Appl. Phys. Lett. **91**, 191904 (2007).
[56]H. Pitkänen, M. Alatalo, A. Puisto, M. Ropo, K. Kokko, M. P. J. Punkkinen, P. Olsson, B. Johansson, S. Hertzman, and L. Vitos, Phys. Rev. B **79**, 024108 (2009).
[57]J. W. Yeh, Y. L. Chen, S. J. Lin, and S. K. Chen, Mater. Sci. Forum **560**, 1 (2007).
[58]M. S. Lucas, G. B. Wilks, L. Mauger, J. A. Munoz, O. N. Senkov, E. Michel, J. Horwath, S. L. Semiatin, M. B. Stone, D. L. Abernathy, and E. Karapetrova, Appl. Phys. Lett. **100**, 251907 (2012).
[59]E. K. Delczeg-Czirjak, E. Nurmi, K. Kokko, and L. Vitos, Phys. Rev. B **84**, 094205 (2011).
[60]K. B. Zhang and Z. Y. Fu, Intermetallics **22**, 24 (2012).
[61]D. Nguyen-Manh, M. Mrovec, and S. P. Fitzgerald, Mater. Trans. **49**, 2497 (2008).
[62]L. Vitos, P. Korzhavyi, and B. Johansson, Nat. Mater. **2**, 25 (2003).
[63]S. F. Pugh, Philos. Mag. **45**, 823 (1954).
[64]X. J. Gu, A. G. McDermott, S. Joseph Poon, and G. J. Shiflet, Appl. Phys. Lett. **88**, 211905 (2006).
[65]F. J. Wang, Y. Zhang, and G. L. Chen, J. Alloys Compd. **478**, 321 (2009).
[66]Y. J. Zhou, Y. Zhang, Y. L. Wang, and G. L. Chen, Appl. Phys. Lett. **90**, 181904 (2007).